Journal of Biomechanics 44 (2011) 337–344

Contents lists available at ScienceDirect

Journal of Biomechanics

journal homepage: www.elsevier.com/locate/jbiomech
www.JBiomech.com

Spectral analysis and connectivity of porous microstructures in bone

Kenneth M. Golden *, N. Benjamin Murphy, Elena Cherkaev

University of Utah, Department of Mathematics, 155 S 1400 E RM 233, Salt Lake City, UT 84112-0090, USA

ARTICLE INFO

Article history:
Accepted 21 October 2010

Keywords:
Bone
Sea ice
Porosity
Percolation
Spectral reconstruction

ABSTRACT

Cancellous bone is a porous composite of calcified tissue interspersed with soft marrow. Sea ice is also a porous composite, consisting of pure ice with brine, air, and salt inclusions. Interestingly, the microstructures of bone and sea ice exhibit notable similarities. In recent years, we have developed mathematical and experimental techniques for imaging and characterizing the brine microstructure of sea ice, such as its volume fraction and connectivity, as well as a range of theoretical approaches for studying fluid, thermal, and electromagnetic transport in sea ice. Here we explore the application of our sea ice techniques to investigate trabecular bone. For example, percolation theory that quantifies brine connectivity and its thermal evolution can also help assess the impact of osteoporosis on trabecular structure. Central to our approach is the *spectral measure* of a composite material, which contains detailed information about the mixture geometry, and can be used in powerful integral representations to compute the effective properties. The spectral measure is obtained from the eigenvalues and eigenvectors of a self-adjoint operator determined exclusively by the composite microgeometry. Here we compute the spectral measures for discretizations of images of healthy and osteoporotic bone. The measures are used to compute the effective electromagnetic properties of the bone specimens. These data are then inverted to reconstruct the porosity of the original specimens, with excellent agreement.

1. Introduction

Bone displays a complex, porous microstructure whose characteristics depend on its macrostructure, whether cortical or cancellous, as well as age and health of the individual. The strength of bone and its ability to resist fracture depend strongly on this porous microstructure, and in particular, on the *quality* of the connectedness of the hard, solid phase (Odgaard, 1997; Kabel et al., 1999; Hollister et al., 1994). For example, in dense cortical bone the pores can be sparse and disconnected, yet exhibit increasing volume fraction and connectivity with the onset of osteoporosis. Cancellous bone displays a broad range of biconnected microstructures, ranging from a solid network of connected trabeculae containing numerous connected pores, to sparse solid fibers within a dominant, connected pore space. With the onset of osteoporosis, cancellous bone can become more disconnected and remaining connections can become more tenuous or fragile. There have been many studies of bone structure (including porosity) and mechanics, and how they depend on aging and other factors (Ural and Vashishth, 2006; Fritsch and Hellmich, 2007; Nalla et al., 2004; Hildebrand et al., 1999; Coelho et al., 2009; Burghardt et al., 2010; Hollister et al., 1994).

In this paper we consider what percolation theory, or the mathematical theory of connectedness, can tell us about bone structure. In particular, we investigate the spectral measures for two examples of porous bone microstructure. A spectral measure is the key mathematical object appearing in integral representations for effective transport and elastic properties of two phase composites (Golden and Papanicolaou, 1983; Kantor and Bergman, 1984). It contains, in principle, most of the geometrical information about the composite. For example, the mass of the measure is the porosity, or volume fraction of one phase, and the absence of large-scale connectivity is associated with a gap in the spectrum. Here we intend to introduce methods of analyzing bone microstructure and its properties which may eventually help in clinical applications. Steps in this direction have been taken already in (Bonifasi-Lista and Cherkaev, 2005, 2008, 2009; Bonifasi-Lista et al., 2009), where *inverse homogenization theory* (Cherkaev, 2001; Cherkaeva and Golden, 1998) has been extended to the evaluation of bone structure, which is discussed in detail below.

Here we observe that some of the natural questions we ask about sea ice, as well as the methods to address them, are also relevant for studies of bone (Fig. 1). For sea ice we have applied percolation theory to understand the thermal evolution of the brine microstructure and its connectedness (Golden et al., 1998a, 2007; Pringle et al., 2009). We have also developed X-ray CT imaging methods and pore structure analysis (Golden et al., 2007; Pringle et al., 2009) to investigate the microstructure and verify our earlier conjecture of a connectedness and fluid transport transition at a

* Corresponding author. Tel.: +1 801 581 6176; fax: +1 801 581 4148.
E-mail address: golden@math.utah.edu (K.M. Golden).

0021-9290/$ - see front matter © 2010 Elsevier Ltd. All rights reserved.
doi:10.1016/j.jbiomech.2010.10.029

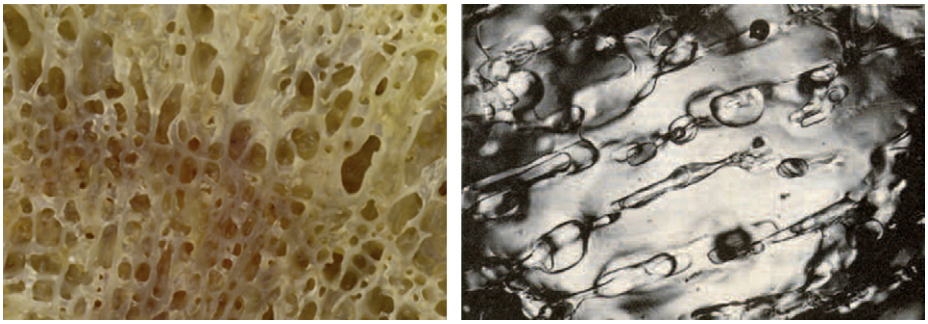

Fig. 1. The porous microstructure in the proximal femur of a 52-year old female with normal bone density is shown on the left (photo courtesy of Maria-Grazia Ascenzi). The brine inclusions in sea ice are shown on the right.

brine volume fraction of about 5%, which corresponds to a critical temperature of $-5\,^{\circ}$C for a typical bulk salinity of 5 parts per thousand, known as the *rule of fives* (Golden et al., 1998a). In studying the role of sea ice in the climate system, we are then interested in how this complex microstructure determines the fluid (Golden et al., 2007) and thermal transport properties of sea ice. The electromagnetic properties of sea ice with applications to remote sensing have been studied extensively in Golden (1995a, 1997a), Golden et al. (1998b,1998c) and Gully et al. (2007). An overview is given by Golden (2009). Microstructural imaging and characterization of bone (Fritsch and Hellmich, 2007; Hildebrand et al., 1999; Kazakia et al., 2008; Issever et al., 2009; Burghardt et al., 2010) is fundamental to studies of its effective mechanical properties (Ural and Vashishth, 2006; Nalla et al., 2004; Oyen et al., 2008; Coelho et al., 2009; Hollister et al., 1994), as well as its fluid (Piekarski and Munro, 1977; Anderson and Knothe Tate, 2008; Knothe Tate et al., 2009), electromagnetic (Sierpowska et al., 2003; Singh and Saha, 1984; Saha and Williams, 1992; Williams and Saha, 1996), and thermal (Davidson and James, 2000; Biyikli et al., 1986) transport properties.

It should be mentioned that there have been other mathematical approaches to characterizing the connectivity of trabecular architecture and its relation to bone quality and strength. In particular, there has been substantial research focused on using the so-called *Euler–Poincaré characteristic*, an integral geometrical quantity, to provide an estimate of the connectivity of the pore space structure (Odgaard and Gundersen, 1993; Odgaard, 1997; Kabel et al., 1999; Jinnai et al., 2002; Roque et al., 2009). An important aspect of this characteristic is that it does not change under deformation or scaling of an object—it is a topological invariant which has been investigated to distinguish between osteoporotic and healthy bone. The percolation and spectral characterization of bone microstructure presented here is more statistical in nature, rooted in issues of long range order and connectedness, and motivated by statistical mechanics and the theory of random composites. Understanding the relations between our approach and the Euler–Poincaré characteristic is a topic for future research.

2. Mathematical methods

2.1. Analytic continuation and the spectral measure

Homogenization denotes a field of applied mathematics where the goal is to find a homogeneous medium which behaves macroscopically just like a given inhomogeneous medium. We briefly describe the analytic continuation method for studying the effective properties of composite materials (Bergman, 1980; Milton, 1980; Golden and Papanicolaou, 1983; Golden, 1997a), or for homogenizing inhomogeneous media. Let $\varepsilon(x,\omega)$ be a spatially stationary random field in $x \in \mathbb{R}^d$, where d is spatial dimension, and $\omega \in \Omega$, where Ω is the set of all realizations of the random medium, which represents the local values of the complex permittivity. This key parameter is defined in basic electromagnetism and determines the propagation properties of an electromagnetic wave in a medium. The real part represents the polarizability of the medium, and the imaginary part the losses. We assume $\varepsilon(x)$ (where we suppress the ω notation) takes the values ε_1 in bone marrow and ε_2 in bone, where both of these parameters depend on frequency, and write $\varepsilon(x) = \varepsilon_1(1-\chi(x)) + \varepsilon_2\chi(x)$, where χ is the characteristic function of the bone, which equals one for all realizations $\omega \in \Omega$ having bone at x, and equals zero otherwise. Let $E(x)$ and $D(x)$ be the stationary random electric and displacement fields satisfying the constitutive law $D(x) = \varepsilon(x)E(x)$ and the equations

$$\nabla \cdot D = 0, \quad \nabla \times E = 0, \tag{1}$$

with $\langle E(x) \rangle = e_k$, where e_k is a unit vector in the kth direction for some $k = 1, \ldots, d$, and $\langle \cdot \rangle$ means an ensemble average over Ω or spatial average over all of $\mathbb{R}^d$.

The effective complex permittivity tensor $\boldsymbol{\varepsilon}^*$ is defined by

$$\langle D \rangle = \boldsymbol{\varepsilon}^* \langle E \rangle. \tag{2}$$

Without loss of generality, we focus on one diagonal coefficient $\varepsilon^* = \varepsilon^*_{kk}$. Due to homogeneity, $\varepsilon^*(a\varepsilon_1, a\varepsilon_2) = a\varepsilon^*(\varepsilon_1, \varepsilon_2)$, for any complex number a, ε^* depends only on the ratio $h = \varepsilon_2/\varepsilon_1$, and we define $m(h) = \varepsilon^*/\varepsilon_1$. The two main properties of $m(h)$ are that it is analytic off $(-\infty, 0]$ in the h-plane, and that it maps the upper half plane to the upper half plane, so that it is an example of a Herglotz, or Stieltjes function. The key step in the analytic continuation method is obtaining an integral representation for ε^*.

It is more convenient to work with the function $F(s) = 1 - m(h)$, where $s = 1/(1-h)$, which is analytic off [0,1] in the s-plane. It was proven (Golden and Papanicolaou, 1983; Bergman, 1978) that $F(s)$ has the representation

$$F(s) = \int_0^1 \frac{d\mu(\lambda)}{s-\lambda}, \quad s \notin [0,1], \tag{3}$$

where μ is a positive measure on [0,1]. This formula arises from the resolvent representation of the electric field $E = s(s+\Gamma\chi)^{-1}e_k$, where $\Gamma = \nabla(-\Delta)^{-1}\nabla\cdot$ and $\Delta = \nabla^2$ is the Laplacian, yielding

$$F(s) = \langle \chi[(s+\Gamma\chi)^{-1}e_k] \cdot e_k \rangle. \tag{4}$$

In the Hilbert space $L^2(\Omega)$ with weight χ in the inner product, $\Gamma\chi$ is a bounded self-adjoint operator. Formula (3) is the spectral representation of the resolvent, and μ is a *spectral measure* of $\Gamma\chi$, in the e_k state. The integral representation (3) separates the parameter information in s from information about the mixture geometry contained in μ. Statistical assumptions about the geometry are incorporated into μ via its moments $\mu_n = \int_0^1 \lambda^n \, d\mu(\lambda)$, which can be calculated from the correlation functions of the random medium, with

$$\mu_n = (-1)^n \langle \chi[(\Gamma\chi)^n e_k] \cdot e_k \rangle. \tag{5}$$

The mass μ_0 is the bone volume fraction ϕ (with $1-\phi$ the porosity),

$$\mu_0 = \int_0^1 d\mu(z) = \langle \chi \rangle = \phi. \tag{6}$$

A principal application of the analytic continuation method is to derive *forward bounds* on ε^* given partial information on the microgeometry (Bergman, 1980; Milton, 1980; Golden, 1997a; Golden et al., 1998c; Gully et al., 2007). The objective of *inverse bounds* is to use data about the electromagnetic response of a composite to bound its structural parameters such as ϕ (Cherkaeva and Golden, 1998; Golden et al., 1998b; McPhedran et al., 1982; McPhedran and Milton, 1990; Cherkaeva and Tripp, 1996; Tripp et al., 1998). Below we will use a more sophisticated inversion scheme over frequency to reconstruct the spectral measure, and obtain accurate estimates of bone volume fraction ϕ. A powerful application of this inverse homogenization approach (Cherkaev, 2001) is that once the spectral measure has been reconstructed, it can be used to calculate other effective properties such as DC electrical conductivity or thermal conductivity, which have analogous integral representations. Thus, through this spectral coupling, other transport properties can be estimated indirectly from EM monitoring (Cherkaev, 2001, 2003; Cherkaev and Zhang, 2003).

2.2. Reconstruction of the spectral measure

The problem of extracting microstructural information from bulk property measurements was introduced previously by McPhedran et al. (1982) and McPhedran and Milton (1990). They estimated the volume fraction of one component in a two phase mixture from measurements of the effective complex permittivity of the composite material. An analytical approach to estimating the volume fractions of materials in a composite was developed (Cherkaeva and Tripp, 1996; Tripp et al., 1998), and extended to the problem of finding bounds on the microstructural parameters for isotropic composite materials by Cherkaeva and Golden (1998). The analytical method is based on the integral representation in (3) and gives explicit formulas for bounds on the volume fraction of one of the constituents (Cherkaeva and Golden, 1998).

The problem of characterizing microstructural information from effective property measurements was formulated as an inverse problem for the spectral measure μ in the Stieltjes analytic representation (Cherkaev, 2001). Uniqueness of the reconstruction of the spectral measure (Cherkaev, 2001) gives a basis for the theory of inverse homogenization. The spectral measure μ in the integral representation (or spectral function) can be uniquely reconstructed if measurements of the effective properties of the composite are available along an arc in the complex s-plane (Cherkaev, 2001). Such data can be obtained from measurements in an interval of frequency provided that at least one of the constituents is frequency dependent.

The numerical problem of reconstructing the spectral function is ill-posed, that is, the solution is highly sensitive to changes in the data, and requires regularization (Cherkaev, 2001). Several regularized algorithms have been developed (Cherkaev, 2001, 2003; Cherkaev and Zhang, 2003). To obtain a stable reconstruction of the spectral measure, an inversion method based on constrained rational approximation of the spectral function was developed by Zhang and Cherkaev (2008, 2009).

The inverse homogenization method was extended to the viscoelastic problem by Bonifasi-Lista and Cherkaev (2005, 2008) for torsion of a cylinder whose microstructure does not change in the axial direction. With this simplified model of bone, this method was used successfully to recover porosity from measurements of the effective shear modulus simulated using micro-CT images of cancellous bone (Bonifasi-Lista and Cherkaev, 2008; Bonifasi-Lista et al., 2009). An electrical impedance spectroscopy method developed by Bonifasi-Lista and Cherkaev (2009) shows potential for reconstructing bone porosity from effective electrical measurements. The method is based on reconstruction of the spectral function from electrical measurements and calculating the zeroth moment, which gives the volume fraction of one of the bone components (Bonifasi-Lista and Cherkaev, 2009). The method was applied to the effective electrical properties of cancellous bone, and numerically calculated using micro-CT images of human vertebrae to find the bone porosity. It was shown that bone porosity can be accurately reconstructed even in the presence of errors in the measured data and uncertainty in the properties of bone and bone marrow.

The problem of reconstructing the spectral measure μ can be reduced to an inverse potential problem. It was shown by Cherkaev (2001) that $F(s)$ admits a representation as a logarithmic potential of the measure μ:

$$F(s)=\frac{\partial \Phi}{\partial s}, \quad \Phi(s)=\int_0^1 \ln|s-\lambda|\, d\mu(\lambda), \tag{7}$$

where $\partial/\partial s=\partial/\partial x-i\partial/\partial y$. The potential Φ solves the Poisson equation $-\Delta\Phi=\rho$, where $\rho(\lambda)$ is a density on [0,1]. A solution to the forward problem is given by the Newtonian potential with $\mu(d\lambda)=\rho(\lambda)\, d\lambda$. The inverse problem is to find $\rho(\lambda)$ (or μ) given values of Φ, $\partial\Phi/\partial n$, or $\nabla\Phi$.

To construct the solution to the inverse problem we formulate the related minimization problem:

$$\min_{\mu}||A\mu-F||, \tag{8}$$

where $A\mu=(\partial/\partial s)\int_0^1 \ln|s-\lambda|\, d\mu(\lambda)$, the norm is the L^2-norm, and F is the given function of the measured data, $F(s)=1-\varepsilon^*(s)/\varepsilon_1$, $s\in\mathbb{C}$. The solution of the problem does not depend continuously on the data. Unboundedness of the operator A^{-1} leads to arbitrarily large variations in the solution, and the problem requires a regularization technique.

A regularization algorithm developed by Cherkaev (2001) is based on constrained minimization. It introduces a stabilization functional which constrains the set of minimizers. As a result, the solution depends continuously on the input data. Instead of minimizing (8) over all functions, the minimization is performed over a convex subset of functions, which results in a stable reconstruction algorithm. The stabilization functional added to the minimization functional in (8), with regularization parameter α, was chosen (Cherkaev, 2001; Bonifasi-Lista and Cherkaev, 2009) as a quadratic functional corresponding to Tikhonov regularization. We use this approach here as wel.

2.3. Percolation theory

Lattice and continuum percolation theories (Stauffer and Aharony, 1992; Torquato, 2002; Hornung, 1997) have been used to model a broad range of disordered materials where the connectedness of one phase dominates effective behavior. Consider the square ($d=2$) or cubic ($d=3$) network of bonds joining nearest neighbor sites on the integer lattice $\mathbb{Z}^d$. We consider the problem of electrical transport through the network. The bonds are assigned electrical conductivities $\sigma_0>0$ (open) or 0 (closed) with probabilities p and $1-p$. Groups of connected open bonds are called open clusters, and the average cluster size grows as p increases. The striking feature of this model is that there is a critical probability p_c, $0<p_c<1$, called the *percolation threshold*, where an infinite cluster of open bonds first appears. In $d=2$, $p_c=\frac{1}{2}$, and in $d=3$, $p_c\approx 0.25$. Typical configurations for the $d=2$ square lattice above and below the threshold are shown in Fig. 2. Near the threshold, or transition point, the order parameters of the system, such as the infinite cluster density, the correlation length, and the effective conductivity are characterized by universal critical exponents which depend only on dimension, and not on the details of the lattice.

An important feature of phase transitions in statistical mechanics, such as in the Ising model of a ferromagnet (Thompson, 1988), is the collapse of a spectral gap as the critical point is approached (Baker, 1990, 1968). Similarly, there is a gap in the support of the spectral measure for p below p_c (Clerc et al., 1990; Day and Thorpe, 1996; Golden, 1997b, 1995b; Jonckheere and Luck, 1998), which collapses as the threshold is approached.

3. Results

3.1. Numerical calculation of the spectral measure for bone

In Section 2 we discussed how the effective properties of a composite such as bone may be expressed in terms of the spectral measure μ of a self-adjoint operator $\Gamma\chi$, where χ is the indicator function for the bone and $\Gamma=\nabla(-\Delta)^{-1}\nabla\cdot$ acts as a projector onto curl free fields. We observed that $\Gamma\chi$ is a self-adjoint operator with respect to the inner product with weight χ. Here it is more convenient to use the standard L^2 inner product and consider the self-adjoint operator $\chi\Gamma\chi$ (the two approaches are easily seen to be equivalent). In order to identify bone microstructures with spectral measures, we have set threshold levels and then discretized two SEM images of trabecular bone from http://hansmalab.physics.ucsb.edu. The first image, shown

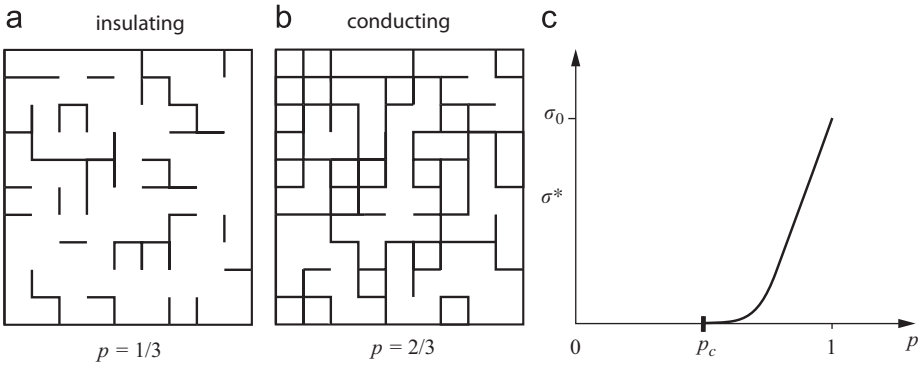

Fig. 2. The two-dimensional square bond lattice below its percolation threshold $p_c=1/2$ in (a), and above its threshold in (b). Below p_c, there is no bulk transport, and above p_c the transport coefficient takes off with power law behavior, as shown in (c).

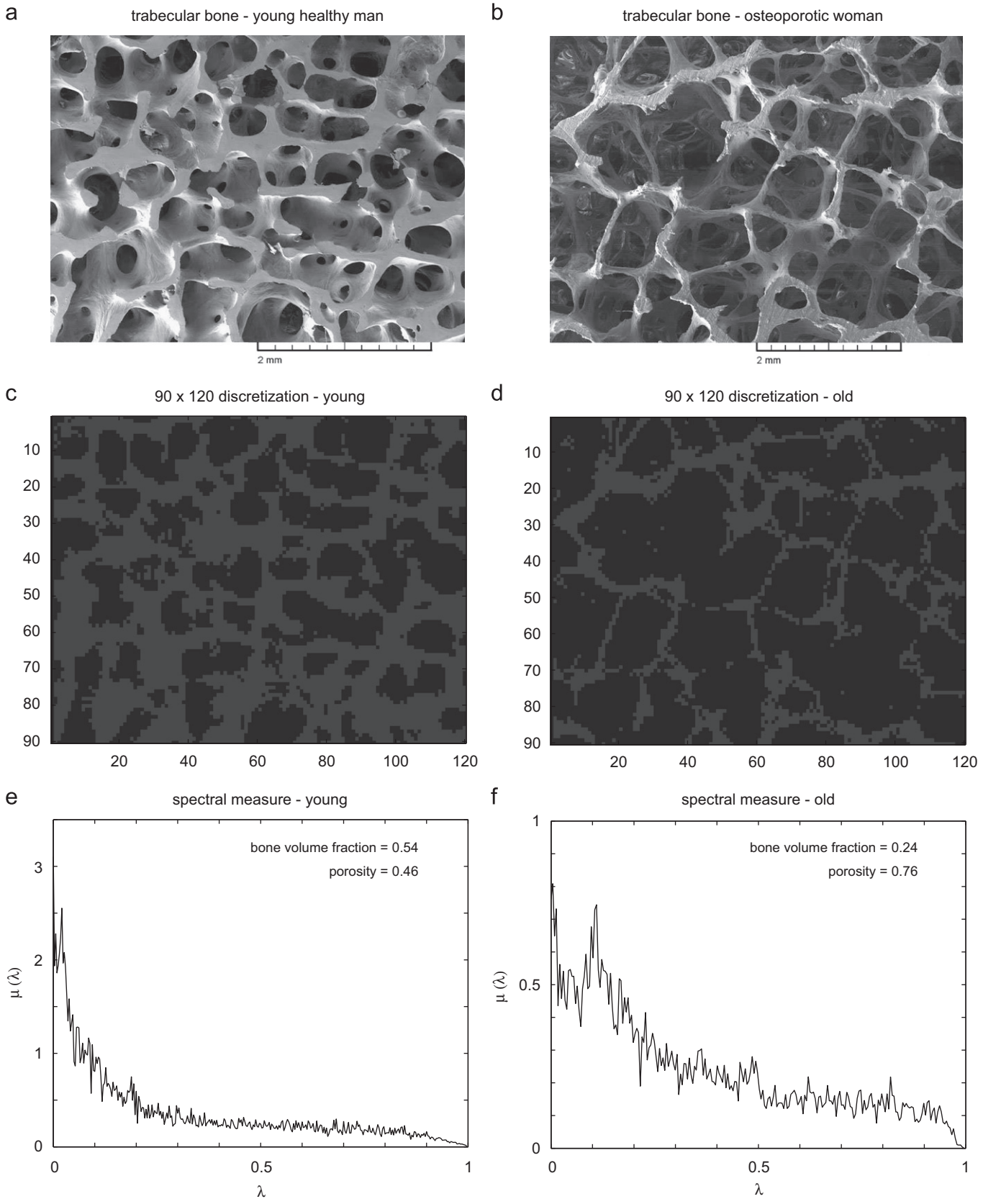

Fig. 3. SEM images of healthy and osteoporotic trabecular bone are shown in (a) and (b), respectively, and their coarsened lattice discretizations are shown in (c) and (d). The graphs of the associated spectral functions are shown in (e) and (f). The spectral functions have been normalized by the uniform bin size so that the area under each graph represents the mass ϕ of the spectral measure, or the bone volume fraction.

in Fig. 3a, is from a young (22-year old) healthy adult man. The second, shown in Fig. 3b, is from an elderly, osteoporotic woman in her eighties. Discretizations of these images are shown in Fig. 3c and d. We remark that the images in Fig. 3a and b are three-dimensional, but our discretizations are two-dimensional representations (surface slices) of the underlying images. Our subsequent calculations of the spectral measure are then two-dimensional as well.

The discretizations are associated with networks of 1's (bone) and 0's (marrow), as in the two-dimensional square lattice percolation model, in order to calculate the corresponding spectral measures. On this square lattice the action of the differential operators ∇ and $\nabla\cdot$ are defined in terms of the forward and backward difference operators (Golden, 1992). Furthermore, the action of χ is that of a square diagonal matrix with ones and zeros along the diagonal corresponding to type two bonds (bone) and type one bonds (marrow), respectively. Therefore the action of the self-adjoint operator $\chi\Gamma\chi$ on this lattice is given by that of a real symmetric matrix, and the spectral measure may be calculated directly from its eigenvalues $\{\lambda_i\}$ and eigenvectors $\{v_i\}$ via the formula

$$d\mu(\lambda) = \sum_{i=1}^{n} m_i \delta(\lambda-\lambda_i)\, d\lambda, \quad m_i = \langle e_0^T v_i v_i^T e_0 \rangle, \tag{9}$$

where $\delta(\lambda)$ is the Dirac delta function and e_0 is a vector of ones. The effective complex permittivity is given by

$$F(s) = \sum_i \frac{m_i}{s-\lambda_i}, \quad \varepsilon^* = \varepsilon_1(1-F(s)), \tag{10}$$

where $s = 1/(1-\varepsilon_2/\varepsilon_1)$.

As the system size N increases, the size of the matrix n increases proportionally by N^2, and the eigenvalues become increasingly dense in the spectral interval [0,1]. For a random system averaged over many realizations (or using a large-enough spatial sample of a fixed realization), a high resolution histogram of the spectral measure begins to resemble a smooth curve, as in Fig. 4c and d. The presence or absence of spectral gaps at the endpoints of the spectral interval and the details of how large the gap is or how large the spectral values m_i are at the collapse give important information pertaining to the connectivity and electromagnetic transport properties of the system.

We have approximated the two-dimensional geometric structure in pictures of sliced healthy and osteoporotic trabecular bone by a 540×540 square lattice bond network. The CPU time for solving the spectral problem for a given square sample grows like N^6. We have optimized the use of our algorithm by averaging over six coarser discretizations of the original 540×540 discretizations. Each of the 90×90 coarser representations sample every 6th data point of the original 540×540 system with a shifted starting point, sampling every data point of the fine mesh 540×540 discretization. As in Jonckheere and Luck (1998), where the spectral measure was obtained by an indirect method, in our method of calculating the spectral measure, we separate the calculation of the delta function at the left endpoint $\lambda = 0$ from the calculation of the spectral measure in the rest of the interval. In order to see the details of the spectral measure throughout the interval, we avoid plotting the delta function at $\lambda = 0$.

The spectral measures for healthy and osteoporotic bone are shown in Fig. 3e and f, respectively. The actual bone volume fractions in the discretized images are 0.5386 and 0.2431, respectively. For comparison, in Fig. 4a and b we show realizations of the 30×30 percolation model with $p = 0.5$ and 0.25, respectively, along with direct calculations of the spectral measures (averaged over 5000 statistical samples) in c and d. The graphs show linearly connected peaks of histograms with bin sizes on the order of 10^{-2}.

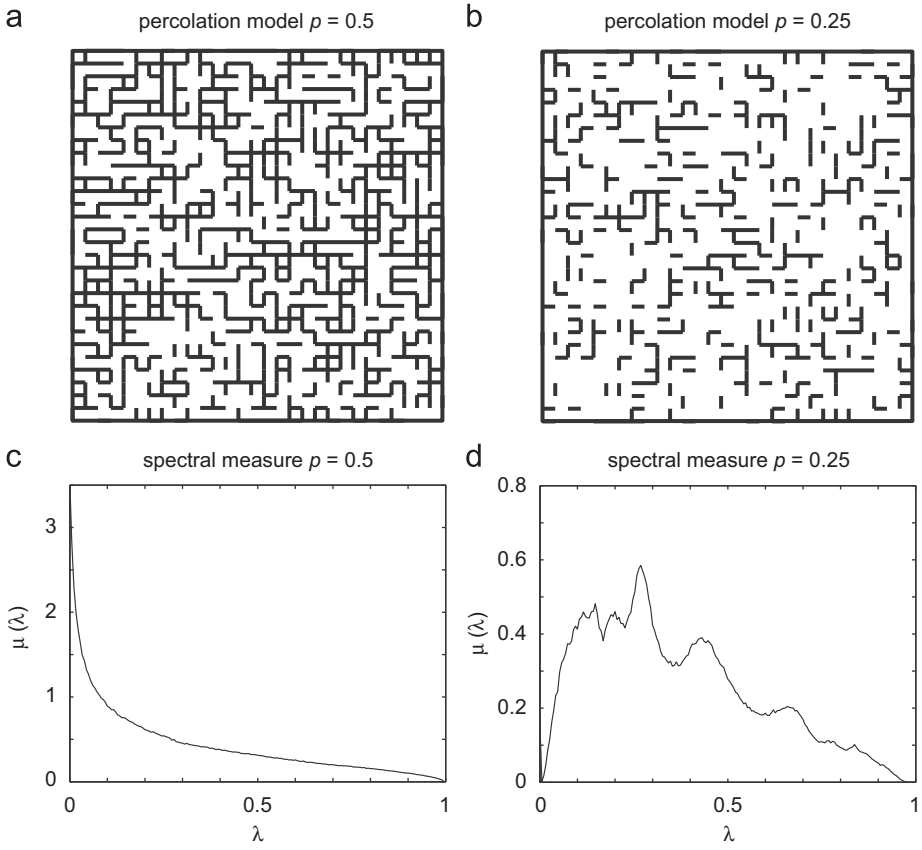

Fig. 4. Realizations of the two-dimensional lattice percolation model are shown in (a) and (b), and the corresponding spectral functions (averaged over 5000 random realizations) are shown in (c) and (d). In (d), there is a spectral gap around $\lambda = 1$, indicating the lack of long-range order or connectedness. The gap collapses in (c) when the percolation threshold of $p = p_c = 0.5$ has been reached, and the system exhibits long-range connectedness. Note the difference in vertical scale in the graphs in (c) and (d).

The function constructed in this way from the weights m_i in the spectral measure is called the *spectral function* $\mu(\lambda)$, and provides a graphical representation of the measure. The apparent smoothness of the spectral function graphs corresponding to the random bond networks is due to the large number ($\sim 10^6$) of eigenvalues and eigenvectors calculated. In contrast, the jaggedness of the spectral function graphs corresponding to the discretizations of trabecular bone is due to the relatively small number ($\sim 10^4$) of eigenvalues and eigenvectors calculated. In order to reveal the detail of the spectral functions with $p=0.5$ for the lattice model and for the young bone, we have limited the plot domain to $(\eta, 1-\eta)$ with $\eta \sim 10^{-15}$, eliminating some of the divergent behavior in the graph. No such restriction was necessary for the spectral functions with $p=0.25$ for either the lattice model or the old bone.

In Fig. 5 (from Golden et al., 2007) we show how the connectedness of the brine microstructure in sea ice changes dramatically with small changes in temperature. If trabecular connectedness behaved similarly, an individual could develop osteoporosis from a fever!

3.2. Numerical inversion for the spectral measure

To simulate the effective complex permittivity of the sample, we used data on the permittivity of bone and bone marrow in Gabriel et al. (1996a,1996b), and calculated the values of $F(s)$ for a set of points in the s-plane. Some of the data in the s-plane used in the reconstruction are shown in Fig. 6. The reconstructed spectral functions are shown in Fig. 7. We use dashed curves to indicate the results obtained for the old bone, and solid curves to show the spectral functions corresponding to young bone. We plot two curves in each case for reconstructions using the real or imaginary parts of the integral operator A.

The porosity of the samples was estimated as the zeroth moment of the spectral measure. We averaged the values over a range of the regularization parameter α to avoid the problem of choosing its appropriate value. We did not add any additional noise to the data, however, the results obtained by Bonifasi-Lista and Cherkaev (2009) indicate that by using this approach, the values of the porosity can be stably recovered from the effective properties, even in the presence of large noise. In Bonifasi-Lista and Cherkaev (2009), an L-curve method was used to find an optimal value of the parameter α, the regularized method used a Tikhonov stabilization functional.

4. Discussion

Properties of the spectral measure provide valuable information about the structure of trabecular bone and the degradation in the quality of connectedness as osteoporosis progresses. Interestingly, we observe that the spectral function for young, healthy bone with volume fraction $\phi \approx 0.54$ in Fig. 3e closely resembles the spectral function for the lattice percolation model with $p=0.5$. Both geometries exhibit long-range connectedness, and this is reflected in the absence of a spectral gap in both cases. However, for the osteoporotic bone with volume fraction $\phi \approx 0.24$, its spectral function shown in Fig. 3f does not have an obvious gap as in the corresponding lattice model with $p=0.25$. While the lattice model is below its percolation threshold, the bone is still connected over the scale of the image, even if the connections are tenuous or fragile, and the gap is not present. The tenuousness of the connections is nevertheless manifested by a sudden decrease in the height of the spectral function from $m_i \sim 10^{-6}$ for $1-\lambda_i \lesssim 10^{-3}$ to $m_i \sim 10^{-35}$ for $1-\lambda_i \gtrsim 10^{-3}$. Therefore, even though the gap has effectively collapsed, the weakness of the connection is manifested in the spectral function. Due to these tenuous connections the spectral function of osteoporotic trabecular bone has characteristics of both of the random networks shown in Fig. 4.

For our reconstructions of the spectral measure, estimates of the bone volume fraction obtained by averaging the zeroth moment of the spectral measures reconstructed with $\alpha = 0.1, 0.01, 0.001$ give excellent agreement with the values calculated from the images.

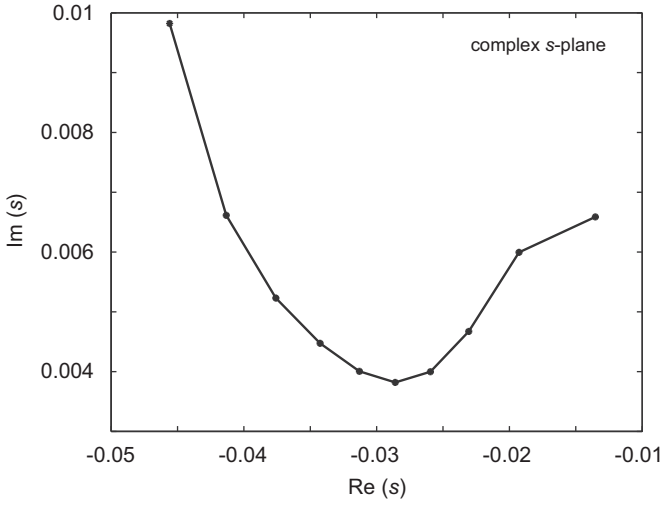

Fig. 6. Data points in the complex s-plane, where $s = 1/(1-\varepsilon_2/\varepsilon_1)$, ε_1 is the complex permittivity of marrow, and ε_2 is the complex permittivity of bone. Both of these parameters depend on the frequency of the applied electric field, and the values of s form an arc in the complex plane as the frequency is varied over the range from 10 Hz to 100 GHz, although only the lower part of this range is shown here.

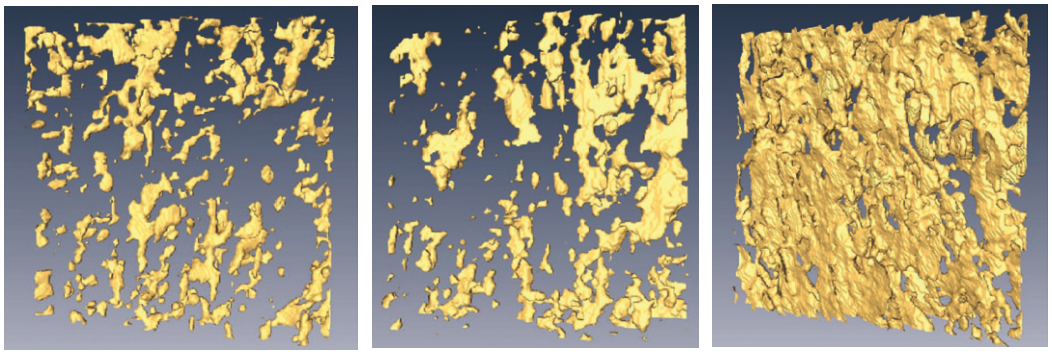

Fig. 5. Thermal evolution of X-ray CT images of the brine phase within a lab-grown sea-ice single crystal with salinity of 9.3 ppt. The (non-collocated) $8 \times 8 \times 2$ mm volumes illustrate a pronounced change in the micro-scale morphology and connectivity of the brine inclusions during warming. As the sample warms beyond the percolation threshold at a brine volume fraction ϕ of about 0.05, the images show the development of long-range order, in the form of connected pathways which facilitate transport.

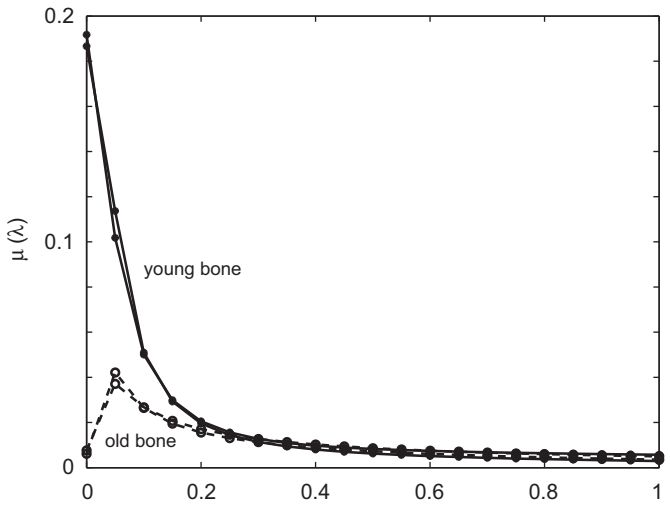

Fig. 7. Reconstruction of the spectral function using the Tikhonov regularization method. The dashed curves denote reconstructions for the old bone, and the solid curves show the recovered spectral function for the young bone. For these reconstructions, the values have not been normalized by the bin size as in Figs. 3 and 4, so that the bone porosity is not obtained by the area under the curve, but by the sum of the reconstructed spectral data points. Also, the bin size here is much larger than in Fig. 3, which explains the discrepancies in the details of the graphs.

For young and old bone samples, the true bone volume fraction was calculated as 0.5386 and 0.2431, and the reconstructed values were 0.5384 and 0.2418, respectively. Other features of the reconstructed spectral functions for the young bone agree well with the spectral function in Fig. 3e. The reconstructed spectral function for the older bone, however, shows some discrepancy with Fig. 3f. While the zeroth moments match up very closely, we believe that the different behavior near $\lambda = 0$ may be due to the much larger bin size used for the reconstructions. Such issues will be investigated further in subsequent work.

We remark that the validity of our approach can be tested experimentally. The spectral measure for a bone specimen can be calculated as we have here from microstructural imagery. Then using this measure in an integral representation for an effective material property, such as the complex permittivity or electrical conductivity, the predicted material property could be compared with experimental measurements of the same property. In this regard, while we have computed the spectral measure here only in two dimensions, the method extends easily to three dimensions, although the numerical calculations are significantly more intensive and time consuming.

In conclusion, we have introduced a new way of characterizing the porous microstructure in bone. We have applied our methods to specimens of trabecular bone, although the same approach can be applied to the porous microstructure of cortical bone as well. A particular strength of focusing on a spectral characterization of the microstructure as we have here is that the spectral measure is precisely what enters into calculations of material properties. On the other hand, it is not clear at this stage how to obtain very specific, small scale information about the microstructure, such as the sizes or shapes of the trabeculae from the spectral measure. This represents a limitation of our current approach, and an interesting area for future research.

Conflict of interest statement

The authors declare that there are no conflicts of interest associated with this work.

Acknowledgments

We are very grateful for the support provided by the Division of Mathematical Sciences and the Arctic Natural Sciences Program at the US National Science Foundation (NSF). Ben Murphy was supported by an NSF VIGRE graduate fellowship, which is gratefully acknowledged. We would also like to thank David Dobson, who wrote an early version of the program which computes the spectral measure, and Maria-Grazia Ascenzi for her help in providing numerous bone images as well as with the manuscript.

References

Anderson, E.J., Knothe Tate, M.L., 2008. Idealization of pericellular fluid space geometry and dimension results in a profound underprediction of nano-microscale stresses imparted by fluid drag on osteocytes. J. Biomech. 41, 1736–1746.
Baker, G.A., 1990. Quantitative Theory of Critical Phenomena. Academic Press, New York.
Baker, G.A., 1968. Some rigorous inequalities satisfied by the ferromagnetic Ising model in a magnetic field. Phys. Rev. Lett. 20, 990–992.
Bergman, D.J., 1978. The dielectric constant of a composite material—a problem in classical physics. Phys. Rep. C 43 (9), 377–407.
Bergman, D.J., 1980. Exactly solvable microscopic geometries and rigorous bounds for the complex dielectric constant of a two-component composite material. Phys. Rev. Lett. 44, 1285.
Biyikli, S., Modest, M.F., Tarr, R., 1986. Measurements of thermal properties for human femora. J. Biomed. Mater. Res. 20 (9), 1335–1345.
Bonifasi-Lista, C., Cherkaev, E., 2005. Identification of bone microstructure from effective complex modulus. In: Inan, E., Kiris, A. (Eds.), Vibration Problems. Springer Proceedings in Physics, vol. 111; 2005, pp. 91–96.
Bonifasi-Lista, C., Cherkaev, E., 2008. Analytical relations between effective material properties and microporosity: application to bone mechanics. International Journal of Engineering Science 46, 1239–1252.
Bonifasi-Lista, C., Cherkaev, E., 2009. Electrical impedance spectroscopy as a potential tool for recovering bone porosity. Phys. Med. Biol. 54, 3063–3082.
Bonifasi-Lista, C., Cherkaev, E., Yeni, Y.N., 2009. Analytical approach to recovering bone porosity from effective complex shear modulus. J. Biomech. Eng. 131, 121003-1–121003-8.
Burghardt, A.J., Kazakia, G.J., Ramachandran, S., Link, T.M., Majumdar, S., 2010. Age- and gender-related differences in the geometric properties and biomechanical significance of intracortical porosity in the distal radius and tibia. J. Bone Miner. Res. 25 (5), 983–993.
Cherkaev, E., 2001. Inverse homogenization for evaluation of effective properties of a mixture. Inverse Problems 17, 1203–1218.
Cherkaev, E., 2003. Spectral coupling of effective properties of a random mixture. In: Movchan, A.B. (Ed.), IUTAM Symposium on Asymptotics, Singularities and Homogenisation in Problems of Mechanics. Kluwer Academic Press, pp. 331–340.
Cherkaev, E., Zhang, D., 2003. Coupling of the effective properties of a random mixture through the reconstructed spectral representation. Physica B 338, 16–23.
Cherkaeva, E., Golden, K.M., 1998. Inverse bounds for microstructural parameters of composite media derived from complex permittivity measurements. Waves Random Media 8 (4), 437–450.
Cherkaeva, E., Tripp, A.C., 1996. Bounds on porosity for dielectric logging. In: Proceedings of the Ninth Conference of the European Consortium for Mathematics in Industry, ECMI 96, Danish Technical University, 1996, pp. 304–306.
Clerc, J.P., Giraud, G., Laugier, J.M., Luck, J.M., 1990. The electrical conductivity of binary disordered systems, percolation clusters, fractals and related models. Adv. Phys. 39 (3), 191–309.
Coelho, P.G., Fernandes, P.R., Rodrigues, H.C., Cardoso, J.B., Guedes, J.M., 2009. Numerical modeling of bone tissue adaptation—a hierarchical approach for bone apparent density and trabecular structure. J. Biomech. 42, 830–837.
Davidson, S.R.H., James, D.F., 2000. Measurement of thermal conductivity of bovine cortical bone. Med. Eng. Phys. 22 (10), 741–747.
Day, A.R., Thorpe, M.F., 1996. The spectral function of random resistor networks. J. Phys. Condens. Matter 8, 4389–4409.
Fritsch, A., Hellmich, C., 2007. Universal microstructural patterns in cortical and trabecular, extracellular and extravascular bone materials: micromechanics-based prediction of anisotropic elasticity. J. Theor. Biol. 244, 597–620.
Gabriel, C., Gabriel, S., Corthout, E., 1996a. The dielectric properties of biological tissues: I. Literature survey. Phys. Med. Biol. 41, 2231–2249.
Gabriel, S., Lau, R.W., Gabriel, C., 1996b. The dielectric properties of biological tissues: II. Measurements in the frequency range 10 hz to 20 GHz. Phys. Med. Biol. 41, 2251–2269.
Golden, K., 1992. Exponent inequalities for the bulk conductivity of a hierarchical model. Commun. Math. Phys. 43 (3), 467–499.
Golden, K., 1995a. Bounds on the complex permittivity of sea ice. J. Geophys. Res. (Oceans) 100 (C7) 13,699–13,711.
Golden, K., Papanicolaou, G., 1983. Bounds for effective parameters of heterogeneous media by analytic continuation. Commun. Math. Phys. 90, 473–491.

Golden, K.M., 1997a. The interaction of microwaves with sea ice. In: Papanicolaou, G. (Ed.), Wave Propagation in Complex Media, IMA Volumes in Mathematics and its Applications, vol. 96. Springer-Verlag, pp. 75–94.
Golden, K.M., 1995b. Statistical mechanics of conducting phase transitions. J. Math. Phys. 36 (10), 5627–5642.
Golden, K.M., 2009. Climate change and the mathematics of transport in sea ice. Not. Am. Math. Soc. 56 (5), 562–584 and issue cover.
Golden, K.M., 1997b. Critical behavior of transport in lattice and continuum percolation models. Phys. Rev. Lett. 78 (20), 3935–3938.
Golden, K.M., Ackley, S.F., Lytle, V.I., 1998a. The percolation phase transition in sea ice. Science 282, 2238–2241.
Golden, K.M., Borup, D., Cheney, M., Cherkaeva, E., Dawson, M.S., Ding, K.H., Fung, A.K., Isaacson, D., Johnson, S.A., Jordan, A.K., Kong, J.A., Kwok, R., Nghiem, S.V., Onstott, R.G., Sylvester, J., Winebrenner, D.P., Zabel, I., 1998b. Inverse electromagnetic scattering models for sea ice. IEEE Trans. Geosci. Remote Sens. 36 (5), 1675–1704.
Golden, K.M., Cheney, M., Ding, K.H., Fung, A.K., Grenfell, T.C., Isaacson, D., Kong, J.A., Nghiem, S.V., Sylvester, J., Winebrenner, D.P., 1998c. Forward electromagnetic scattering models for sea ice. IEEE Trans. Geosci. Remote Sens. 36 (5), 1655–1674.
Golden, K.M., Eicken, H., Heaton, A.L., Miner, J., Pringle, D., Zhu, J., 2007. Thermal evolution of permeability and microstructure in sea ice. Geophys. Res. Lett. 34, L16501. doi:10.1029/2007GL030447 (6 pages and issue cover).
Gully, A., Backstrom, L.G.E., Eicken, H., Golden, K.M., 2007. Complex bounds and microstructural recovery from measurements of sea ice permittivity. Physica B 394, 357–362.
Hildebrand, T., Laib, A., Müller, R., Dequeker, J., Rüegsegger, P., 1999. Direct three-dimensional morphometric analysis of human cancellous bone: Microstructural data from spine femur iliac crest and calcaneus. J. Bone Miner. Res. 14 (7), 1167–1174.
Hollister, S.J., Brennan, J.M., Kikuchi, N., 1994. A homogenization sampling procedure for calculating trabecular bone effective stiffness and tissue level stress. J. Biomech. 27 (4), 433–444.
Hornung, U. (Ed.), Homogenization and Porous Media. Springer, New York, 1997.
Issever, A.S., Link, T.M., Kentenich, M., Rogalla, P., Schwieger, K., Huber, M.B., Burghardt, A.J., Majumdar, S., Diederichs, G., 2009. Trabecular bone structure analysis in the osteoporotic spine using a clinical in vivo setup for slice mdct imaging: comparison to μct imaging and μfe modeling. J. Bone Miner. Res. 24 (9), 1628–1637.
Jinnai, H., Watashiba, H., Kajihara, T., Nishikawa, Y., Takahashi, M., Ito, M., 2002. Surface curvatures of trabecular bone microarchitecture. Bone 30 (1), 191–194.
Jonckheere, T., Luck, J.M., 1998. Dielectric resonances of binary random networks. J. Phys. A Math. Gen. 31, 3687–3717.
Kabel, J., Odgaard, A., van Rietbergen, B., Huiskes, R., 1999. Connectivity and the elastic properties of cancellous bone. Bone 24 (2), 115–120.
Kantor, Y., Bergman, D.J., 1984. Improved rigorous bounds on the effective elastic moduli of a composite material. J. Mech. Phys. Solid 32 (1), 41–62.
Kazakia, G.J., Hyun, B., Burghardt, A.J., Krug, R., Newitt, D.C., de Papp, A.E., Link, T.M., Majumdar, S., 2008. In vivo determination of bone structure in postmenopausal women: a comparison of hr-pqct and high-field mr imaging. J. Bone Miner. Res. 23 (4), 463–474.
Knothe Tate, M.L., Steck, R., Anderson, E.J., 2009. Bone as an inspiration for a novel class of mechanoactive materials. Biomaterials 30, 133–140.
McPhedran, R.C., Milton, G.W., 1990. Inverse transport problems for composite media. Mater. Res. Soc. Sympos. Proc. 195, 257–274.
McPhedran, R.C., McKenzie, D.R., Milton, G.W., 1982. Extraction of structural information from measured transport properties of composites. Appl. Phys. A 29, 19–27.
Milton, G.W., 1980. Bounds on the complex dielectric constant of a composite material. Appl. Phys. Lett. 37, 300–302.
Nalla, R.K., Kruzica, J.J., Kinney, J.H., Ritchie, R.O., 2004. Effect of aging on the toughness of human cortical bone: evaluation by R-curves. Bone 35, 1240–1246.
Odgaard, A., 1997. Three-dimensional methods for quantification of cancellous bone architecture. Bone 20 (4), 315–328.
Odgaard, A., Gundersen, H.J.G., 1993. Quantification of connectivity in cancellous bone, with special emphasis on 3-d reconstructions. Bone 14 (2), 173–182.
Oyen, M.L., Ferguson, V.L., Bembey, A.K., Bushby, A.J., Boyd, A., 2008. Composite bounds on the elastic modulus of bone. J. Biomech. 41, 2585–2588.
Piekarski, N., Munro, M., 1977. Transport mechanism operating between blood supply and osteocytes in long bones. Nature 269, 80–82.
Pringle, D.J., Miner, J.E., Eicken, H., Golden, K.M., 2009. Pore-space percolation in sea ice single crystals. J. Geophys. Res. (Oceans) 114 (C12017).
Roque, W.L., Carlos, A., de Souza, A., Barbieri, D.X., 2009. The Euler–Poincaré characteristic applied to identify low bone density from vertebral tomographic images. Rev. Bras. Reumatol. 49 (2), 140–152.
Saha, S., Williams, P.A., 1992. Electric and dielectric properties of wet human cortical bone as a function of frequency. IEEE Trans. Biomed. Eng. 39 (12), 1298–1304.
Sierpowska, J., Töyräs, J., Hakulinen, M.A., Saarakkala, S., Jurvelin, J.S., Lappalainen, R., 2003. Electrical and dielectric properties of bovine trabecular bone–relationships with mechanical properties and mineral density. Phys. Med. Biol. 48, 775–786.
Singh, S., Saha, S., 1984. Electrical properties of bone. A review. Clin. Orthop. Relat. Res. 186, 249–271.
Stauffer, D., Aharony, A., 1992. Introduction to Percolation Theory, second ed. Taylor and Francis Ltd, London.
Thompson, C.J., 1988. Classical Equilibrium Statistical Mechanics. Oxford University Press, Oxford.
Torquato, S., 2002. Random Heterogeneous Materials: Microstructure and Macroscopic Properties. Springer-Verlag, New York.
Tripp, A.C., Cherkaeva, E., Hulen, J., 1998. Bounds on the complex conductivity of geophysical mixtures. Geophys. Prospect. 46, 589–601.
Ural, A., Vashishth, D., 2006. Cohesive finite element modeling of age-related toughness loss in human cortical bone. J. Biomech. 39, 2974–2982.
Williams, P.A., Saha, S., 1996. The electrical and dielectric properties of human bone tissue and their relationship with density and bone mineral content. Ann. Biomed. Eng. 24 (2), 222–233.
Zhang, D., Cherkaev, E., 2008. Padé approximations for identification of air bubble volume from temperature or frequency dependent permittivity of a two-component mixture. Inverse Problems Sci. Eng. 16 (4), 425–445.
Zhang, D., Cherkaev, E., 2009. Reconstruction of spectral function from effective permittivity of a composite material using rational function approximations. J. Comput. Phys 228, 5390–5409.